



Generator-coordinate methods with symmetry-restored Hartree-Fock-Bogoliubov wave functions for large-scale shell-model calculations

Noritaka Shimizu ^{1,*}, Takahiro Mizusaki,² Kazunari Kaneko,³ and Yusuke Tsunoda ¹

¹Center for Nuclear Study, The University of Tokyo, Hongo, Bunkyo-ku, Tokyo 113-0033, Japan

²Institute of Natural Sciences, Senshu University, 3-8-1 Kanda-Jinbocho, Chiyoda-ku, Tokyo 101-8425, Japan

³Department of Physics, Kyushu Sangyo University, Fukuoka 813-8503, Japan



(Received 20 March 2021; accepted 25 May 2021; published 3 June 2021)

The generator coordinate method (GCM) combined with the projection method is applied to large-scale shell-model calculations. The quadrupole deformation is taken as a generator coordinate and the GCM basis states are prepared by the quadrupole-constrained Hartree-Fock Bogoliubov method with the variation after particle-number projection. The resultant GCM wave function is a linear combination of the angular-momentum and parity projected basis states. We discuss how well the present method approximates the exact solution of the shell-model diagonalization method by the benchmark tests of ⁴⁸Ca, ⁵⁶Ni, and ⁴⁸Cr in the *pf*-shell model space and those of ¹³²Ba and ¹³³Ba in the $50 < N, Z < 82$ model space.

DOI: [10.1103/PhysRevC.103.064302](https://doi.org/10.1103/PhysRevC.103.064302)

I. INTRODUCTION

Solving the quantum many-body problem is one of the hardest challenges in modern physics. In the development of computational many-body approaches to the investigation of nuclear structures, two directions have been largely explored: one is to pursue the exact solution in a rather small model space and the other is to search for mean-field approaches and their extensions in a comparably large single-particle space. The nuclear shell-model calculations have belonged mainly to the former. They were numerically solved by exact diagonalization in their earliest years, especially for light nuclei, and have seemed to be incompatible with mean-field approaches because the single-particle space is too small to consider the mean field. For the latter, the generator coordinate method (GCM) has been developed beyond the mean-field method. Especially, the GCM combined with the full angular-momentum projection method has recently been developed with the energy density functional theory [1–4] and has also been applied to antisymmetrized molecular dynamics [5]. Moreover, it has been successfully applied to large-scale shell-model calculations with realistic shell-model residual interactions. To clarify the circumstances so far, we briefly review the historical development of the shell-model calculations.

In the 1970s and 1980s, a conventional shell-model diagonalization method was developed, and systematic studies of the *sd* shell were achieved [6]. In the 1990s, shell-model studies entered into *pf*-shell nuclei, which were investigated enthusiastically by using various truncation schemes. Several realistic interactions for *pf*-shell nuclei were suggested [7–9]. However, toward the middle of the *pf* shell, the exact diagonalization method has faced the dimensional problem of

the shell model space, and 2 million was the largest record for state-of-the-art shell-model calculations in 1995 [10]. The maximum dimension of the full *pf* shell reaches about 2×10^9 in the *M* scheme. The shell-model dimension grows in a combinatorial way by distributing protons and neutrons in the shell-model orbits. It was apparent that the diagonalization approach is limited by the combinatorial explosion of the dimension. On the other hand, from the early 1990s, a new trend has begun to emerge in which large-scale shell-model calculations are carried out as precisely as possible beyond the limit of conventional diagonalization by Monte Carlo or variational methods, i.e., the shell-model Monte Carlo (SMMC) [11], the Monte Carlo shell model (MCSM) [12], and series of VAMPIR approaches [13]. By making full use of state-of-the-art computer resources, these approaches have successfully opened new ground and widened the horizon.

Around 2000, shell-model calculations became feasible in the *pf* shell and larger ones, and the reachable size of the model was increased drastically. More light has thereby been shed on the mean-field aspect of shell-model calculations. The GCM equipped with the full angular-momentum projection has helped analyze the ingredients of shell-model wave functions. For example, the GCM with an axially or triaxially deformed Hartree-Fock (HF) wave function has been utilized to discuss shape coexistence and backbending phenomena [14–16]. The GCM method with Nilsson-BCS wave functions was also discussed in the single-*j* shell model [17]. The next step is clearly to carry out the GCM with the angular-momentum projected Hartree-Fock-Bogoliubov (HFB) basis as shell-model calculations, while there was a known phase determination of the Onishi formula in the full angular-momentum projected HFB [18]. This problem was, however, completely solved with the Pfaffian by Robledo [19].

After his epochal work, we developed an angular-momentum projected GCM with the HFB basis state, and

*shimizu@cns.s.u-tokyo.ac.jp

we found that it gave good excitation energies for the pf shell as partially shown in Ref. [20]. We have applied this method to studies of the shape evolution of Nd isotopes [21] and of $N \sim Z$ nuclei [22] for the PMMU Hamiltonian, which is a schematic interaction based on the pairing plus QQ with monopole interactions designed for various model spaces [23,24]. A similar GCM method was recently introduced to shell-model calculations combined with the Hamiltonian provided by the valence-shell in-medium similarity renormalization-group method [25–27]. This method was also applied to realistic shell-model interactions [28]. Extension of the GCM by introducing the Tamm-Dancoff mode was also pursued [29].

In the present work, we discuss the details of the angular-momentum projected GCM with the HFB basis states obtained by the particle-number variation after projection (HFB + GCM) with the realistic shell-model Hamiltonian. Especially we demonstrate how well it approximates the exact results and how useful it is for analyzing the collectivity of the wave function. We further discuss the feasibility of the HFB + GCM method in comparison with the HF + GCM and exact diagonalization methods. This paper is organized as follows: the theoretical framework is introduced in Sec. II, the benchmark tests are demonstrated in Sec. III, and the paper is summarized in Sec. IV.

II. THEORETICAL FRAMEWORK

In the conventional GCM, the trial wave function is expressed as a superposition of the generated wave functions, which are labeled by the collective coordinates. In the present work, we always apply the angular-momentum projection to these wave functions for precise description of low-lying excited states. We refer to this angular-momentum projected GCM simply as the GCM hereafter. We take the number-projected HFB wave function as a basis state of the GCM (HFB + GCM), while we also use the Hartree-Fock wave function as a basis state (HF + GCM) for comparison. The general framework of the GCM is described in Sec. II A, and the number-projected HFB wave function for the GCM basis state is discussed in Sec. II B.

A. Generator coordinate method

We briefly review the theoretical framework of the GCM in this section. The GCM wave function is a linear combination of the angular-momentum projected basis states and written as

$$|\Psi^{I\pi}\rangle = \sum_{\alpha,K} f_{\alpha,K}^{I\pi} P_{MK}^{I\pi} |\phi_{\alpha}\rangle, \quad (1)$$

where $f_{\alpha,K}^{I\pi}$ and $P_{MK}^{I\pi}$ are the coefficients of the superposition and the angular-momentum (I) and parity (π) projector, respectively. The details of the GCM framework and the angular-momentum projector are given in Refs. [18,30]. The basis state $|\phi_{\alpha}\rangle$ is a number-projected HFB wave function or a Hartree-Fock wave function parameterized by a set of collective coordinates α , which is often taken as the quadrupole deformation and is described further in Sec. II B.

To evaluate the energy and the amplitude $f_{\alpha,K}^{I\pi}$, the Hamiltonian matrix is diagonalized in the subspace spanned by the angular-momentum and parity projected basis states. They are obtained by solving the generalized eigenvalue problem, or the Hill-Wheeler-Griffin equation [31],

$$\sum_{\beta,K} (\mathcal{H}_{\alpha M,\beta K}^{I\pi} - E^{I\pi} \mathcal{N}_{\alpha M,\beta K}^{I\pi}) f_{\beta K}^{I\pi} = 0 \quad (2)$$

with

$$\mathcal{H}_{\alpha M,\beta K}^{I\pi} = \langle \phi_{\alpha} | H P_{MK}^{I\pi} | \phi_{\beta} \rangle, \quad (3)$$

$$\mathcal{N}_{\alpha M,\beta K}^{I\pi} = \langle \phi_{\alpha} | P_{MK}^{I\pi} | \phi_{\beta} \rangle. \quad (4)$$

To solve Eq. (2), since the HFB basis states are not orthogonal, we diagonalize the norm matrix $\mathcal{N}_{\alpha M,\beta K}^{I\pi}$ to orthogonalize these states as

$$\sum_{\beta K} \mathcal{N}_{\alpha M,\beta K}^{I\pi} u_{\beta K,\lambda}^{I\pi} = n_{\lambda}^{I\pi} u_{\alpha M,\lambda}^{I\pi}, \quad (5)$$

where $n_{\lambda}^{I\pi}$ and $u_{\alpha M,\lambda}^{I\pi}$ are the λ th eigenvalue and its eigenvector, respectively. For numerical stability, we omit the basis states whose eigenvalue is smaller than a certain criterion, e.g., 10^{-6} . It gives the orthonormalized basis state

$$|\psi_{\lambda}^{I\pi}\rangle = \sum_{\alpha K} \frac{u_{\alpha K,\lambda}^{I\pi}}{\sqrt{n_{\lambda}^{I\pi}}} P_{MK}^{I\pi} |\phi_{\alpha}\rangle, \quad (6)$$

which is often called a “natural basis.” Thus, the energy eigenvalue of Eq. (2) is obtained by the eigenvalue problem

$$\sum_{\lambda'} \langle \psi_{\lambda}^{I\pi} | H | \psi_{\lambda'}^{I\pi} \rangle g_{\lambda'}^{I\pi} = E^{I\pi} g_{\lambda}^{I\pi}, \quad (7)$$

and the resultant GCM wave function is rewritten as

$$\begin{aligned} |\Psi^{I\pi}\rangle &= \sum_{\lambda} g_{\lambda}^{I\pi} |\psi_{\lambda}^{I\pi}\rangle \\ &= \sum_{\lambda\alpha K} g_{\lambda}^{I\pi} \frac{u_{\alpha K,\lambda}^{I\pi}}{\sqrt{n_{\lambda}^{I\pi}}} P_{MK}^{I\pi} |\phi_{\alpha}\rangle. \end{aligned} \quad (8)$$

The contribution of the α th basis state to the GCM wave function is defined as

$$P^{I\pi}(\alpha) = \left| \sum_{K\lambda} g_{\lambda}^{I\pi} u_{\alpha K,\lambda}^{I\pi} \right|^2, \quad (9)$$

which is often called the “collective wave function” [1,28].

B. Constrained HFB with particle-number variation after projection

For preparing GCM basis states, we mainly adopt the HFB wave function obtained with the particle-number variation after projection and with quadrupole constraints, which is referred to as the “HFB + GCM.” Instead of the HFB basis state, the Q -constrained Hartree-Fock wave function can be used for GCM basis states, which is referred to as the “HF + GCM” [16].

The number-projected HFB basis state for protons is written as

$$|\phi^{(p)}\rangle = P^Z |U^{(p)}, V^{(p)}\rangle, \quad (10)$$

where P^Z is the proton-number projector. The intrinsic HFB wave function $|U, V\rangle$ is defined as

$$\beta_k |U^{(p)}, V^{(p)}\rangle = 0 \quad \text{for any } k, \quad (11)$$

$$\beta_k = \sum_i (V_{ik}^{(p)} c_i^{(p)\dagger} + U_{ik}^{(p)} c_i^{(p)}), \quad (12)$$

where $c_i^{(p)\dagger}$ is a creation operator of the proton single-particle state i . This Bogoliubov quasiparticle state is parameterized by the matrices $U^{(p)}$ and $V^{(p)}$, which satisfy the orthogonalization relations

$$\begin{aligned} U^\dagger U + V^\dagger V &= 1, & U U^\dagger + V^* V^T &= 1, \\ U^T V + V^T U &= 0, & U V^\dagger + V^* U^T &= 0, \end{aligned} \quad (13)$$

so that β_k satisfies the fermion anticommutation relations. In the present work, we do not assume any symmetries, such as angular momentum, parity, and number, for this ‘‘intrinsic’’ wave function $|U, V\rangle$. Note that we take the matrix elements of U and V as complex numbers without any restriction except that the proton-neutron mixing is not included in the quasiparticle. The neutron basis state $|\phi^{(n)}\rangle$ is defined in the same manner, and the total number-projected state is defined as

$$|\phi\rangle = |\phi^{(p)}\rangle \otimes |\phi^{(n)}\rangle. \quad (14)$$

The number projection is defined as

$$P^Z |U^{(p)}, V^{(p)}\rangle = \frac{1}{2\pi} \int_0^{2\pi} d\phi e^{i\phi(\hat{Z}-Z)} |U^{(p)}, V^{(p)}\rangle, \quad (15)$$

where Z and \hat{Z} are the number of active protons and the proton-number operator, respectively. ϕ in Eq. (15) is a gauge angle, and in practice, the range of this integral can be reduced to $(0, \pi)$ by conserving the number parity [18,32]. Numerically, the integral is computed by the summation of the discretized gauge angles.

The Q -constrained Hartree-Fock-Bogoliubov basis state specified by the quadrupole deformations q_0 and q_2 is obtained by minimizing the energy function with quadratic constraint [18] as

$$E(q_0, q_2) = \langle \phi | H | \phi \rangle + \frac{1}{2} \sum_{m=-2}^2 C_m (\langle \phi | \hat{Q}_m | \phi \rangle - q_m)^2, \quad (16)$$

where $q_2 = q_{-2}$, $q_1 = q_{-1} = 0$, $\hat{Q}_m = r^2 Y_m^{(2)}$, and C_m are positive constants and large enough to constrain $\langle \hat{Q}_i \rangle = q_i$. The energy minimization is performed by the conjugate gradient method [33]. In this method, the energy gradient of the number-projected wave function is required and its formula is given in Refs. [34] and [30]. Hereafter, we refer to the HFB method with the particle-number variation after projection as the ‘‘HFB.’’

In addition to the constraint of the quadrupole deformation, we can add J_x as another collective coordinate to describe high-spin states [35]. It is introduced as a quadratic constraint,

$$E(q_0, q_2, j_x) = E(q_0, q_2) + \frac{1}{2} C_{j_x} (\langle \phi | \hat{J}_x | \phi \rangle - j_x)^2, \quad (17)$$

where \hat{J}_x is the x component of the angular-momentum operator and C_{j_x} is taken large enough to keep the condition $\langle \phi | \hat{J}_x | \phi \rangle = j_x$.

In the GCM, we diagonalize the Hamiltonian matrix in the subspace spanned by the basis states parameterized by a set of the collective coordinates $\alpha = (q_0^{(\alpha)}, q_2^{(\alpha)}, j_x^{(\alpha)})$. In the present paper, typically, ~ 50 sets of $\alpha = (q_0^{(\alpha)}, q_2^{(\alpha)})$ are distributed with equal spacing in the (q_0, q_2) space. This method is called the ‘‘HFB + GCM.’’ When axial symmetry is assumed, only q_0 is taken equally spaced with $q_2 = 0$, which is called the ‘‘axial HFB + GCM.’’ $\langle \hat{J}_x \rangle$ is not constrained without special mention.

A framework similar to the present HFB + GCM method was discussed in the preceding work [28] by taking Ca isotopes as examples. In this preceding work, the U and V coefficients in Eq. (12) were restricted to real numbers, while we take them as complex numbers without any assumption in the present work. Although this restriction is reasonable for the time-reversal-invariant intrinsic state, it may deteriorate the approximation of the HFB + GCM result as demonstrated in Sec. III A.

In the case of the HF + GCM, the basis states are prepared by the constrained Hartree-Fock method. Its wave function is expressed as a Slater determinant,

$$|\phi\rangle = \prod_{k=1}^Z \left(\sum_i D_{ik}^{(p)} c_i^{(p)\dagger} \right) \prod_{l=1}^N \left(\sum_j D_{jl}^{(n)} c_j^{(n)\dagger} \right) |-\rangle, \quad (18)$$

which is parameterized by the matrices $D^{(p)}$ and $D^{(n)}$ [14,36]. Although it is computationally less demanding since the number projection is not required, it is not efficient to describe the pairing correlation. The constraint condition is applied in the same way as the constrained HFB method.

III. NUMERICAL RESULTS

In this section, we present some numerical results of the HFB + GCM compared with the exact results. We take ^{48}Ca , ^{56}Ni , and ^{48}Cr with the pf -shell model space and ^{132}Ba and ^{133}Ba with the $jj55$ model space as examples for the benchmark tests. The pf shell consists of the $0f_{7/2}$, $0f_{5/2}$, $1p_{3/2}$, and $1p_{1/2}$ orbits for both protons and neutrons with a ^{40}Ca inert core. The $jj55$ model space consists of the $0g_{7/2}$, $1d_{5/2}$, $1d_{3/2}$, $2s_{1/2}$, and $0h_{11/2}$ orbits for both protons and neutrons with a ^{100}Sn inert core. In order to discuss the differences between the various basis states for the GCM, we introduce the axial HF + GCM, HF + GCM, axial HFB + GCM, and HFB + GCM methods. In the HF + GCM method, both q_0 and q_2 are taken as collective coordinates to include the degree of freedom of triaxial deformation. The axial HF + GCM denotes the GCM with q_0 as a collective coordinate ($q_2 = 0$) and the GCM basis states are generated by the Hartree-Fock method [14]. In the axial HFB + GCM method, the GCM basis states are generated by the Q -constrained HFB and only q_0 is taken as a collective coordinate. The HFB + GCM includes the triaxially deformed basis states.

The KB3G [37], FPD6 [8], and GXPF1A [38] interactions are successful realistic interactions for the pf -shell model space and have been widely used also for benchmark tests. We

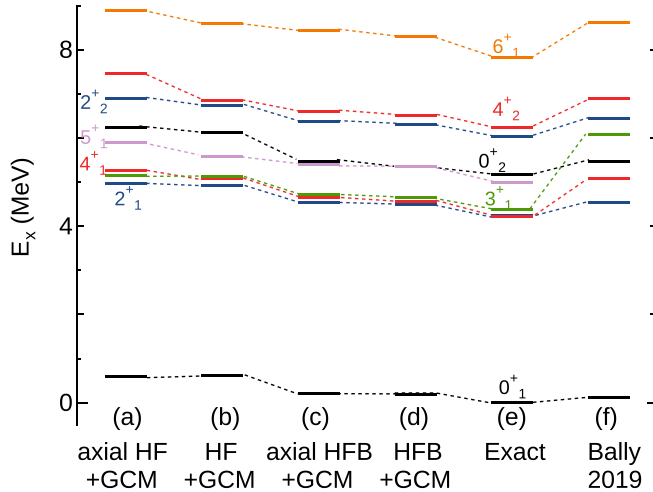


FIG. 1. Excitation energies of the $0_{1,2}^+$ (black), $2_{1,2}^+$ (blue), 3_1^+ (green), $4_{1,2}^+$ (red), 5_1^+ (purple), and 6_1^+ (orange) states of ^{48}Ca relative to the exact ground-state energy with the KB3G interaction [37]. Results obtained by (a) HF + GCM with axial symmetry, (b) HF + GCM, (c) HFB + GCM with axial symmetry, (d) HFB + GCM, (e) exact diagonalization, and (f) the result taken from “PGCM₃” in Ref. [28].

adopt these interactions individually for the benchmark tests of ^{48}Ca , ^{56}Ni , and ^{48}Cr in order to compare our results with literature values and to demonstrate that the difference between these interactions has little impact on the performance of the HFB + GCM.

A. ^{48}Ca with the pf shell

We performed the benchmark test of the GCM calculations taking ^{48}Ca with the KB3G interaction [37] as the first example. The M -scheme dimension of the Hamiltonian matrix is 12 022 and is tractable by the exact diagonalization method. We compare the results of the axial HF + GCM, the HF + GCM, the axial HFB + GCM, and the HFB + GCM, compared with the exact shell-model energies, which were obtained by utilizing the KSHELL code [39]. For the axial HF + GCM and the axial HFB + GCM, we prepare 15 basis states with equally spaced q_0 . For the HF + GCM and the HFB + GCM, we prepare 28 sets of (q_0, q_2) which are equally spaced on the (q_0, q_2) plane.

Figures 1(a)–1(d) show the results obtained by the axial HF + GCM with 15 basis states, the HF + GCM with 28 basis states, the axial HFB + GCM with 15 basis states, and the HFB + GCM with 28 basis states, respectively. These four methods well reproduce the exact shell-model spectrum shown in Fig. 1(e) including the approximate degeneracy of the 2_1^+ , 4_1^+ , and 3_1^+ states. Among them, the HFB + GCM method has the largest variational space and shows the best approximation in view of the variational principle. The differences of the ground-state energies from the exact one are around 200 keV for the axial HFB + GCM and the HFB + GCM, while those for the axial HF + GCM and the HF + GCM are around 600 keV. Figure 1(f) shows the GCM result of Bally and his collaborators [28]. Although it reproduced the

TABLE I. $B(E2)$ transition probabilities ($e^2 \text{fm}^4$) and Q moments ($e \text{fm}^2$) of ^{48}Ca obtained by the HF + GCM, HFB + GCM, and exact diagonalization.

	HF + GCM	HFB + GCM	Exact
$B(E2; 2_1^+ \rightarrow 0_1^+)$	12.1	12.1	11.5
$B(E2; 4_1^+ \rightarrow 2_1^+)$	2.3	2.4	2.0
$B(E2; 4_1^+ \rightarrow 3_1^+)$	9.3	8.4	7.6
$B(E2; 2_2^+ \rightarrow 0_2^+)$	24.9	23.0	21.6
$Q(2_1^+)$	4.3	4.3	4.1
$Q(2_2^+)$	-9.8	-9.2	-8.6
$Q(4_1^+)$	8.4	7.8	7.5
$Q(3_1^+)$	9.7	9.0	8.5

exact spectrum reasonably, it apparently overestimated the 3_1^+ excitation energy. Since the U and V matrices were restricted as real numbers in their work, it would be important to treat these parameters as complex numbers.

The $E2$ reduced transition probabilities obtained by the HF + GCM, the HFB + GCM, and the exact diagonalization method are presented in Table I. The effective charges are taken as $(e_p, e_n) = (1.5, 0.5)e$ throughout this paper. Both the HF + GCM and the HFB + GCM methods show good agreement with the exact one including the Q moment of the 3_1^+ state except that the HF + GCM slightly overestimates the quadrupole collectivity compared to the HFB + GCM and the exact one.

B. ^{56}Ni with the pf shell

In this subsection, we compare the HFB + GCM result to the exact one for ^{56}Ni with the pf -shell model space and the FPD6 interaction [8]. It is a good example for discussing the feasibility and the restriction of the present method, since this system has been used for benchmark tests of various truncation schemes [12–14,30,36,40–42]. The nuclear structure of ^{56}Ni has attracted much attention because of its soft closed core and shape coexistence [14,43,44].

Figure 2 shows the excitation energies of ^{56}Ni with the pf -shell model space in comparison with the exact one. These results were obtained by the HFB + GCM method

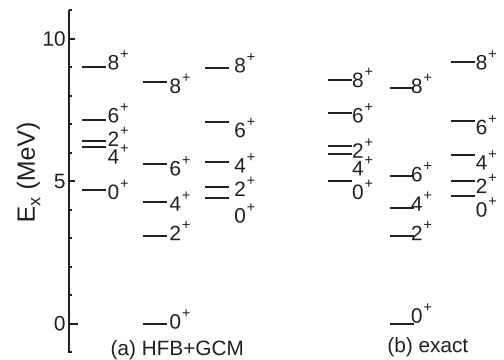


FIG. 2. Excitation energies of ^{56}Ni with the FPD6 interaction [8]. Results obtained by (a) the HFB + GCM method and (b) the exact diagonalization method.

TABLE II. $B(E2)$ transition probabilities ($e^2 \text{fm}^4$) and Q moments ($e \text{fm}^2$) of ^{56}Ni obtained by the HFB + GCM and exact diagonalization.

	HFB + GCM	Exact
$B(E2; 2_1^+ \rightarrow 0_1^+)$	152.3	167.1
$B(E2; 4_1^+ \rightarrow 2_1^+)$	234.0	153.5
$B(E2; 2_2^+ \rightarrow 0_2^+)$	624.2	443.2
$B(E2; 2_3^+ \rightarrow 0_3^+)$	192.7	66.9
$Q(2_1^+)$	27.6	24.2
$Q(4_1^+)$	32.5	26.5
$Q(2_2^+)$	-50.6	-46.5
$Q(2_3^+)$	17.6	12.1

with 55 basis states and the exact diagonalization method (M -scheme dimension, 1 087 455 228). The present HFB + GCM method reproduces the excitation spectrum of the exact ones well. The exact shell-model ground-state energy is $E_{\text{gs}} = -203.198$ keV, while the HFB + GCM method gives $E_{\text{gs}} = -201.549$ MeV. While various methods of the variation after angular-momentum projection, such as the Monte Carlo shell model ($E_{\text{gs}} = -203.152$ MeV) [12], its advanced version ($E_{\text{gs}} = -203.161$ MeV) [40], and the general complex FED VAMPIR approach ($E_{\text{gs}} = -203.119$ MeV) [13], give energies closer to the exact one than the HFB + GCM, these angular-momentum variations after projection generally demand larger computational resources to compute the whole spectrum.

Table II lists the $B(E2)$ transition probabilities and Q moments of ^{56}Ni . While the HFB + GCM method reproduces the exact values reasonably, it overestimates the exact one, especially for the value of the 4^+ state, which might be remedied by introducing the mixing of the proton-neutron pairing in the quasiparticle wave function.

Figure 3 shows the total energy surfaces as a function of the collective coordinates Q_0 and Q_2 . The unprojected energy surface shows the spherical minimum and shallow local minimum at the prolate deformation. Note that “unprojected” means angular-momentum unprojected and the number projection is always performed. In the $J = 0$ projected energy surface, the global minimum is shifted to the oblate deformation.

The GCM wave functions can be analyzed by the collective wave function $P(q_0, q_2)$ defined in Eq. (9). Figure 4 shows the collective wave functions of the 0_1^+ , 0_2^+ , and 0_3^+ states

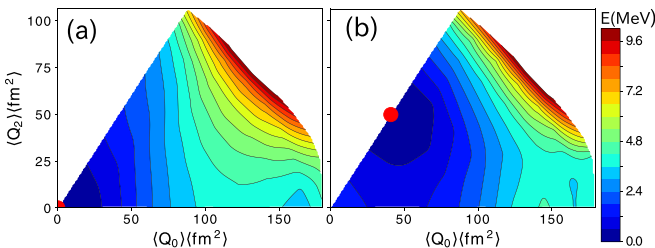


FIG. 3. Total energy surface of ^{56}Ni . (a) Unprojected and (b) $J = 0$ projected energies. Red circles denote the minimum points.

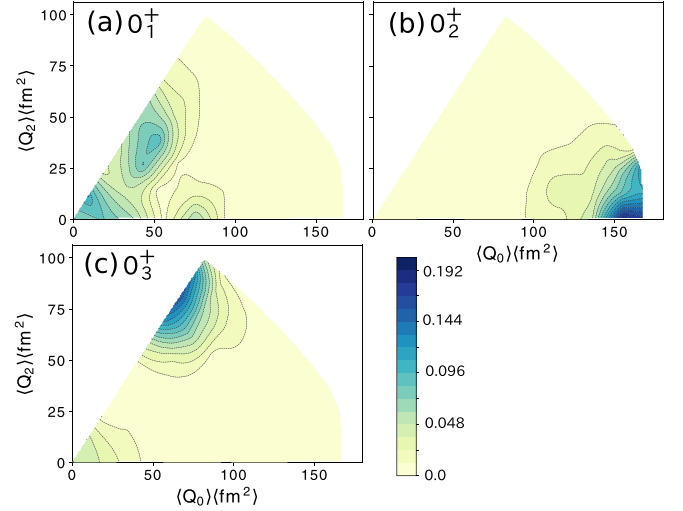


FIG. 4. Collective wave functions of the (a) 0_1^+ , (b) 0_2^+ , and (c) 0_3^+ states of ^{56}Ni obtained by the HFB + GCM.

of ^{56}Ni obtained by the HFB + GCM method. The 0_1^+ state is dominated by the spherical and oblate basis states, which correspond to the global minima of the unprojected surface and the projected energy surface in Fig. 3, respectively. As shown in Fig. 4, the 0_2^+ and 0_3^+ wave functions indicate the prolate and oblate deformations, respectively. Thus, these figures clearly show the shape coexistence of ^{56}Ni , which is consistent with Ref. [14].

C. Backbending of ^{48}Cr

In this subsection, we introduce the cranked basis states to the GCM in order to describe high-spin states more precisely. As an example we take the yrast state of ^{48}Cr , which is known to exhibit the backbending phenomenon [15,16]. The shell-model calculation is performed with the pf -shell model space and the GXPF1A interaction [38]. Figure 5 shows the shell-model results of the γ -ray energies, namely, the energy differences of the yrast J^+ and $(J - 2)^+$ states, of ^{48}Cr . While the γ -ray energy increases as a function of J in general cases of the rotational band, that of ^{48}Cr shows a sudden decrease at $J = 12$. This phenomenon is called backbending and originates from the band crossing [10,15].

While the HFB + GCM result with 21 basis states shows good agreement with the exact one up to $J = 6$, it fails to reproduce the energies at $J \geq 10$ because of the band crossing. To include the higher-band components, we add the constraint $\langle J_x \rangle = \sqrt{I(I + 1)}$ in Eq. (17), with $I = 0, 6$, and 12. We prepare 63 basis states in total and perform the GCM calculation, which is referred to as the “HFB + GCM + Jx” in Fig. 5. This result successfully reproduces the exact ones including the backbending. Thus, the basis states generated by the cranking term are important for describing high-spin states and the band crossing.

D. ^{132}Ba with the $jj55$ model space

As a benchmark of a heavier-mass region than the pf -shell nuclei, we discuss the shell-model results of ^{132}Ba with the

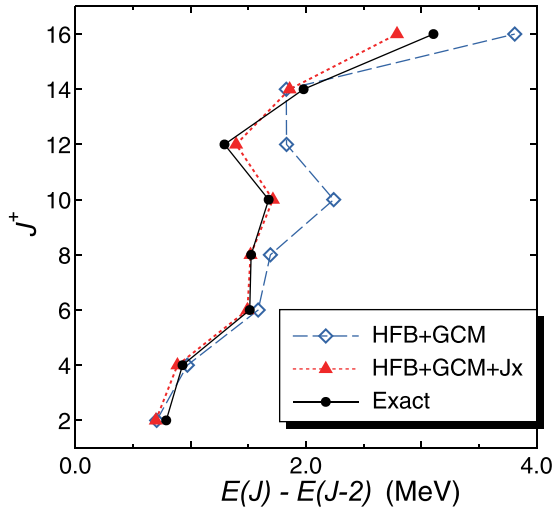


FIG. 5. Gamma-ray energies [$\text{Ex}(J_1^+) - \text{Ex}((J-2)_1^+)$] of ^{48}Cr obtained by the HFB + GCM (open blue diamonds with dashed line), the HFB + GCM + Jx, (filled red triangles with dotted line), and the exact value (filled black circles with solid line).

SN100PN interaction [45] in the $jj55$ model space. Although the M -scheme dimension reaches a huge value, 2.0×10^{10} , the exact diagonalization is still feasible utilizing the KSHELL code and a state-of-the-art supercomputer [39]. ^{132}Ba is considered to be triaxially deformed [46], and its shell-model

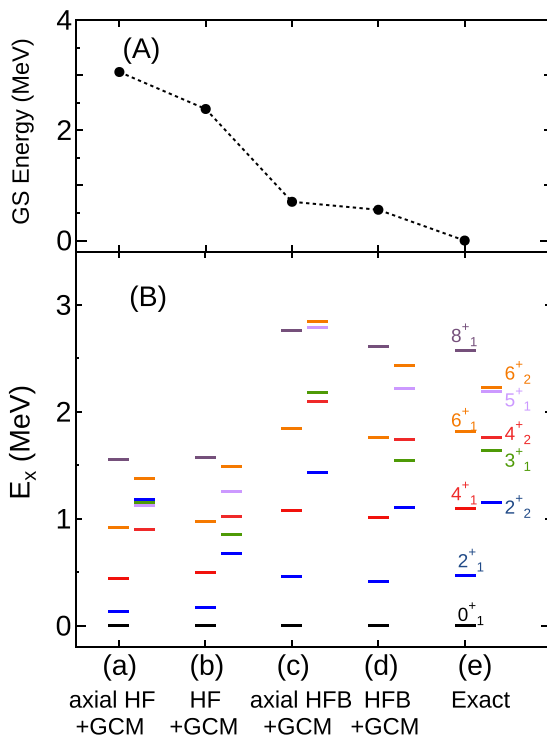


FIG. 6. (A) Ground-state energies relative to the exact one and (B) energy spectra of ^{132}Ba with the SN100PN interaction [45]. Results obtained by (a) axial HF + GCM, (b) HF + GCM, (c) axial HFB + GCM, (d) HFB + GCM, and (e) exact diagonalization.

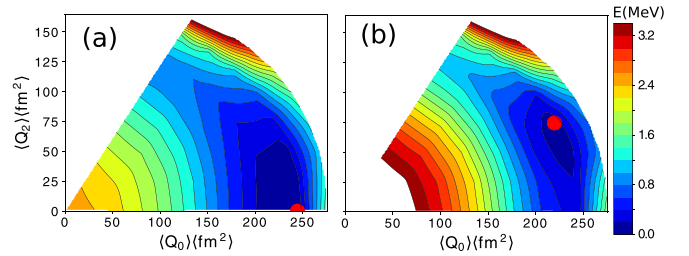


FIG. 7. Total energy surfaces of ^{132}Ba obtained by the quadrupole-constrained HFB with the particle number variation after projection. (a) Unprojected and (b) $J^\pi = 0^+$ projected energy surfaces.

calculation is a good benchmark target to discuss the contribution of the triaxial deformation. We performed the axial HF + GCM and axial HFB + GCM calculations with 19 basis states and the HF + GCM and HFB + GCM calculations with 45 basis states.

The two results provided by the HF + GCM in Figs. 6(a) and 6(b) show level schemes that are too compressed and, thus, overestimate the moment of inertia due to underestimation of the contribution of the pairing correlations by the superposition of the deformed Slater determinants. While the HF + GCM shows the correct ordering of the quasi- γ band, which consists of 2_2^+ , 3_1^+ , 4_2^+ , 5_1^+ , and 6_2^+ states, the axial HF + GCM fails to give its correct ordering.

Figures 6(c) and 6(d) show the results of the axial HFB + GCM and the HFB + GCM, respectively. The HFB basis state enables us to include the pairing correlation appropriately. Although the axial HFB + GCM succeeds in reproducing the ground-state band of the exact result shown in Fig. 6(e), the members of the quasi- γ band are shifted a few hundred keV upward. The HFB + GCM result agrees with the exact one excellently including the quasi- γ band except for the slight overestimation of $E_x(6_2^+)$.

Figure 7 shows the unprojected and $J^\pi = 0^+$ projected energy surfaces of ^{132}Ba . While the unprojected energy sur-

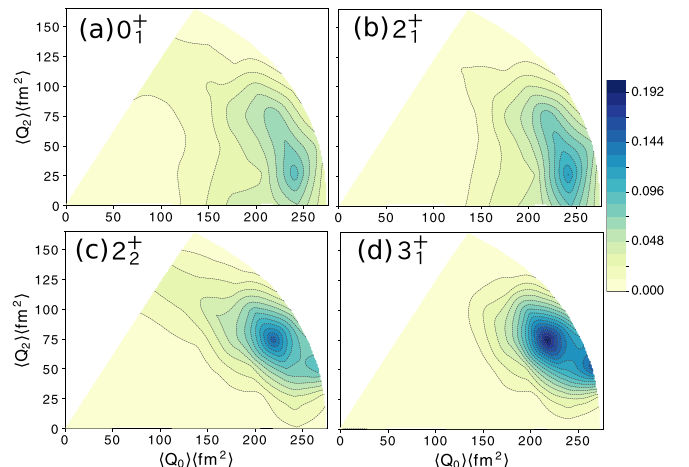


FIG. 8. Collective wave functions of the (a) 0_1^+ , (b) 2_1^+ , (c) 2_2^+ , and (d) 3_1^+ states of ^{132}Ba obtained by the HFB + GCM.

TABLE III. $B(E2)$ transition probabilities ($e^2 \text{fm}^4$) and Q moments ($e \text{fm}^2$) of ^{132}Ba obtained by the HFB + GCM and exact diagonalization.

	HFB + GCM	Exact
$B(E2; 2_1^+ \rightarrow 0_1^+)$	1317	1210
$B(E2; 4_1^+ \rightarrow 2_1^+)$	1972	1820
$B(E2; 2_2^+ \rightarrow 2_1^+)$	777	951
$B(E2; 3_1^+ \rightarrow 2_2^+)$	1999	1780
$Q(2_1^+)$	-59.2	-52.3
$Q(4_1^+)$	-78.4	-74.0
$Q(2_2^+)$	56.6	48.3
$Q(3_1^+)$	0.5	0.8

face shows a prolate minimum with a shallow valley in the γ direction, the $J = 0^+$ projected energy surface has a rigid triaxial minimum. The angular-momentum projection often shifts the axially symmetric minimum to the rigid triaxial minimum, which has been discussed in, e.g., [47–49].

Figure 8 shows the collective wave functions of the 0_1^+ , 2_1^+ , 2_2^+ , and 3_1^+ states of ^{132}Ba obtained by the HFB + GCM. The 0_1^+ and 2_1^+ states, which belong to the ground-state band, show the prolate deformation with modest triaxiality. On the other hand, the 2_2^+ and 3_1^+ states in the quasi- γ band show the rigid triaxial deformation.

Table III shows the $B(E2)$ transition probabilities and Q moments of the low-lying states of ^{132}Ba . The HFB + GCM results reproduce the exact ones successfully. The Q moment of the 3_1^+ state is quite small and exhibits triaxiality, consistent with the triaxial behavior of the collective wave function shown in Fig. 8.

E. ^{133}Ba with the $jj55$ model space

As an example of the applications to odd-mass nuclei, we discuss the HFB + GCM result for ^{133}Ba . The low-lying spectrum of ^{133}Ba was studied experimentally and with shell-model calculations in Ref. [50]. In the present work, the shell-model interaction and the model space are taken to be the same as in the ^{132}Ba case. For the odd-particle system, we keep the intrinsic wave function having an odd number parity [18] and perform particle-number variation after projection. The overlap of the HFB wave functions having odd number parity is calculated following the prescription in

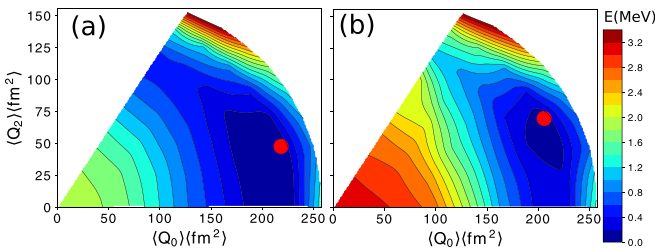


FIG. 9. (a) Unprojected and (b) $J^\pi = 1/2^+$ projected total energy surfaces of ^{133}Ba obtained by the Q -constrained HFB. See caption to Fig. 7 for details.

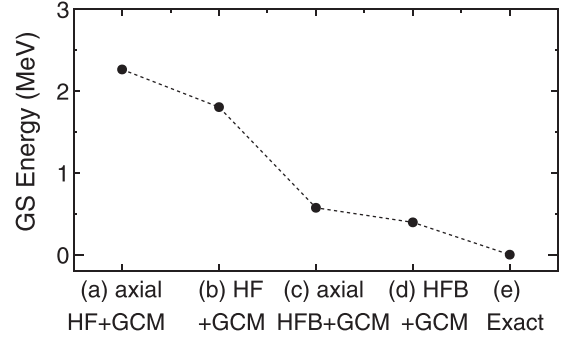


FIG. 10. Ground-state ($1/2_1^+$) energies of ^{133}Ba relative to the exact shell-model energy. See the caption to Fig. 6 for details.

Ref. [51]. The other procedures are the same as in the case of even-even nuclei.

The J^π -unprojected energy surface of ^{133}Ba , presented in Fig. 9(a), has a shallow valley in the γ direction with modest triaxial deformation. The angular-momentum projection shifts the minimum to the rigid triaxial deformation as in Fig. 9(b). This tendency is similar to the ^{132}Ba case.

Figure 10 shows the ground-state energies of the ^{133}Ba obtained by the GCM methods in comparison with the exact shell-model energy. Those of the two HFB + GCM methods are close to the exact value within 500 keV, while the two HF + GCM results have rather large deviations around 2 MeV. They show a similar tendency to the case of ^{132}Ba in Fig. 6(A). The deviation is smaller than in the case of ^{132}Ba , which is reasonable since the M -scheme dimension of ^{133}Ba , 4.5×10^9 , is smaller than that of ^{132}Ba .

Figure 11 shows the energy levels obtained by the HFB + GCM and the exact excitation energies. The HFB + GCM result reproduces the exact one with a roughly 100-keV difference. In comparison with even-even nuclei, the level density tends to increase in odd-mass nuclei, making the variational approximation more difficult.

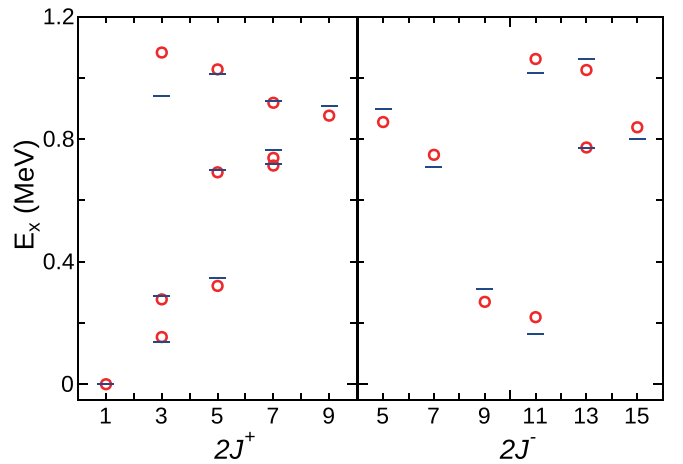


FIG. 11. Energy spectra of ^{133}Ba with the SN100PN interaction [45]. Left: Positive-parity states. Right: Negative-parity states. Results obtained by the HFB + GCM (open red circles) and the exact one (blue lines) vs the total angular momentum $2J$.

TABLE IV. $B(E2)$ transition probabilities ($e^2 \text{fm}^4$) and Q moments ($e \text{fm}^2$) of ^{133}Ba obtained by the HFB + GCM and exact diagonalization.

	HFB + GCM	Exact
$B(E2; 3/2_1^+ \rightarrow 1/2_1^+)$	502	216
$B(E2; 3/2_2^+ \rightarrow 3/2_1^+)$	583	766
$B(E2; 5/2_1^+ \rightarrow 1/2_1^+)$	779	663
$B(E2; 5/2_1^+ \rightarrow 3/2_1^+)$	856	947
$B(E2; 5/2_1^+ \rightarrow 3/2_2^+)$	216	46
$B(E2; 5/2_1^+ \rightarrow 1/2_1^+)$	779	663
$B(E2; 9/2_1^- \rightarrow 11/2_1^-)$	1029	1035
$B(E2; 7/2_1^- \rightarrow 11/2_1^-)$	538	561
$Q(3/2_1^+)$	-32.5	-9.7
$Q(3/2_2^+)$	31.1	8.3
$Q(5/2_1^+)$	-29.0	-26.7
$Q(5/2_2^+)$	-39.7	-34.2
$Q(7/2_1^+)$	49.8	87.2
$Q(7/2_2^+)$	-25.7	-60.8
$Q(11/2_1^-)$	78.8	78.8
$Q(9/2_1^-)$	121.8	117.8
$Q(7/2_1^-)$	28.8	34.4

Table IV presents the $B(E2)$ transition probabilities and Q moments obtained by the HFB + GCM and the exact results. While the HFB + GCM results of the Q moments of the $5/2_1^+$, $5/2_2^+$, $11/2_1^-$, $9/2_1^-$, and $7/2_1^-$ states agree with the exact ones, those of $3/2_1^+$, $3/2_2^+$, $7/2_1^+$, and $7/2_2^+$ show relatively large deviations. Since the excitation energies of the $3/2_1^+$ and $3/2_2^+$ states are close to each other within 150 keV, these two wave functions are suspected to be mixed in the HFB + GCM wave functions. This consideration is supported by the fact that the sum of the Q moments of $3/2_1^+$ and $3/2_2^+$ by the HFB + GCM is close to that of the exact ones. The same situation occurs in the $7/2_1^+$ and $7/2_2^+$ states. If the excitation energies of the yrast and yrare states are close to each other, these two states are prone to be mixed in the HFB + GCM wave functions and the $E2$ transition and Q moment deteriorate. The $B(E2)$ values in Table IV show a similar tendency: while the large discrepancy between the HFB + GCM and the exact ones is seen in the $B(E2)$ values concerning the $3/2^+$ and $7/2^+$ states, the other $B(E2)$ values show a reasonable agreement.

IV. SUMMARY

The HFB + GCM method is investigated as a variational approximation to large-scale shell-model calculations with the conventional diagonalization method. The HFB + GCM is a beyond-mean-field method and is closely related to the total energy surface and projected energy surface as the mean-field approach and its extension. This method is naturally expected to be more prospective in a heavier-mass region with a larger model space, where efficient treatment of the pairing correla-

tion is required. Therefore, it is essential to use model spaces as large as possible for the testing ground. For that purpose, the pf -shell and $jj55$ model spaces were chosen for the benchmark test. In the latter one, state-of-the-art shell-model diagonalization has recently been carried out for some nuclei, and thus verification of the present method is crucial to cover all nuclei in this model space.

We have presented the benchmark tests of the axial HF + GCM, HF + GCM, axial HFB + GCM, and HFB + GCM methods for ^{48}Ca and ^{132}Ba . In the case of ^{48}Ca , the differences among these four methods are relatively small and these methods well reproduce the exact ones. On the other hand, the differences are rather large in the case of ^{132}Ba and only the HFB + GCM method successfully reproduces the exact one including the quasi- γ band since it is necessary to include appropriately both the pairing correlation and the triaxial deformation in this case. Not only the excitation energies but also the $B(E2)$ transition probabilities and Q moments of low-lying states obtained by the HFB + GCM show good agreement with the exact ones. For higher spin states, the $\langle J_x \rangle$ constraint is taken as an additional collective coordinate of the HFB + GCM and its feasibility was demonstrated to describe the backbending structure of ^{48}Cr .

Moreover, we have discussed the HFB + GCM results for ^{56}Ni as an example of shape coexistence and ^{133}Ba as an example of odd-mass nuclei. The collective wave function is drawn for the GCM wave function and is useful to investigate nuclear structures, such as shape coexistence. Although the HFB + GCM gives a reasonable approximation with the results of the exact diagonalization in low-lying states, a rather large discrepancy is seen if two states of the same spin and parity have energies close to each other. Such a situation often occurs in odd-mass nuclei.

We have demonstrated that the HFB + GCM method is a good tool to approximate the exact shell-model result. Since it demands smaller computational resources than the variational approaches after the three-dimensional angular-momentum projection, the present method is a good compromise between the goodness of approximation and the computational costs. The proton-neutron mixing of the quasiparticle vacuum might be important for precisely estimating the nuclear matrix element of neutrinoless double- β decay [52], and this direction of study is in progress.

ACKNOWLEDGMENTS

The numerical calculations were mainly performed on the Oakforest-PACS supercomputer (hp200130, hp190160, hp180179, xg18i035). N.S. and Y.T. acknowledge valuable support by ‘‘Priority Issue on Post-K computer’’ (Elucidation of the Fundamental Laws and Evolution of the Universe) and ‘‘Program for Promoting Researches on the Supercomputer Fugaku’’ (Simulation for Basic Science: From Fundamental Laws of Particles to Creation of Nuclei), MEXT, Japan. N.S. acknowledges KAKENHI Grant No. 17K05433, JSPS, Japan.

[1] R. Rodriguez-Guzman, J. L. Egido, and L. M. Robledo, *Phys. Rev. C* **65**, 024304 (2002).

[2] T. R. Rodriguez and J. L. Egido, *Phys. Rev. Lett.* **99**, 062501 (2007).

- [3] J. L. Egido, M. Borrajo, and T. R. Rodriguez, *Phys. Rev. Lett.* **116**, 052502 (2016).
- [4] T. Nikšić, D. Vretenar, and P. Ring, *Phys. Rev. C* **74**, 064309 (2006).
- [5] M. Kimura and H. Horiuchi, *Phys. Rev. C* **69**, 051304(R) (2004); M. Kimura, *ibid.* **75**, 041302(R) (2007).
- [6] B. A. Brown and B. H. Wildenthal, *Annu. Rev. Nucl. Part. Sci.* **38**, 29 (1988).
- [7] A. Abouzou, E. Caurier, and A. P. Zuker, *Phys. Rev. Lett.* **66**, 1134 (1991).
- [8] W. A. Richter, M. J. Van Der Merwe, R. E. Julies, and B. A. Brown, *Nucl. Phys. A* **523**, 325 (1991).
- [9] E. Caurier, G. Martinez-Pinedo, F. Nowacki, A. Poves, and A. P. Zuker, *Rev. Mod. Phys.* **77**, 427 (2005).
- [10] A. Poves and G. M-Pinedo, *Phys. Lett. B* **430**, 203 (1998).
- [11] S. E. Koonin, D. J. Dean, and K. Langanke, *Phys. Rep.* **278**, 1 (1997).
- [12] T. Otsuka, M. Honma, T. Mizusaki, N. Shimizu, and Y. Utsuno, *Prog. Part. Nucl. Phys.* **47**, 319 (2001).
- [13] K. W. Schmid, *Prog. Part. Nucl. Phys.* **52**, 565 (2004).
- [14] T. Mizusaki, T. Otsuka, Y. Utsuno, M. Honma, and T. Sebe, *Phys. Rev. C* **59**, R1846 (1999).
- [15] K. Hara, Y. Sun, and T. Mizusaki, *Phys. Rev. Lett.* **83**, 1922 (1999).
- [16] T. Mizusaki, T. Otsuka, M. Honma, and B. A. Brown, *Phys. Rev. C* **63**, 044306 (2001).
- [17] K. Enami, K. Tanabe, and N. Yoshinaga, *Phys. Rev. C* **63**, 044322 (2001).
- [18] P. Ring and P. Schuck, *The Nuclear Many-Body Problem* (Springer-Verlag, Berlin, 1980).
- [19] L. M. Robledo, *Phys. Rev. C* **79**, 021302(R) (2009); G. F. Bertsch and L. M. Robledo, *Phys. Rev. Lett.* **108**, 042505 (2012).
- [20] T. Mizusaki, *Bull. INS Senshu Univ.* **47**, 7 (2016) [in Japanese].
- [21] K. Kaneko, N. Shimizu, T. Mizusaki, and Y. Sun, *Phys. Rev. C* **103**, L021301 (2021).
- [22] K. Kaneko, N. Shimizu, T. Mizusaki, and Y. Sun, *Phys. Lett. B* **817**, 136286 (2021).
- [23] K. Kaneko, T. Mizusaki, Y. Sun, and S. Tazaki, *Phys. Rev. C* **89**, 011302(R) (2014).
- [24] K. Kaneko, T. Mizusaki, Y. Sun, and S. Tazaki, *Phys. Rev. C* **92**, 044331 (2015).
- [25] J. M. Yao, J. Engel, L. J. Wang, C. F. Jiao, and H. Hergert, *Phys. Rev. C* **98**, 054311 (2018).
- [26] J. M. Yao, B. Bally, J. Engel, R. Wirth, T. R. Rodriguez, and H. Hergert, *Phys. Rev. Lett.* **124**, 232501 (2020).
- [27] C. F. Jiao, J. Engel, and J. D. Holt, *Phys. Rev. C* **96**, 054310 (2017).
- [28] B. Bally, A. Sanchez-Fernandez, and T. R. Rodriguez, *Phys. Rev. C* **100**, 044308 (2019).
- [29] C. Jiao and C. W. Johnson, *Phys. Rev. C* **100**, 031303(R) (2019).
- [30] N. Shimizu, Y. Tsunoda, Y. Utsuno, and T. Otsuka, *Phys. Rev. C* **103**, 014312 (2021).
- [31] J. J. Griffin and J. A. Wheeler, *Phys. Rev.* **80**, 367 (1966).
- [32] B. Bally and M. Bender, *Phys. Rev. C* **103**, 024315 (2021).
- [33] W. H. Press, B. P. Flannery, S. A. Teukolsky, and W. T. Vetterling, *Numerical Recipes in Fortran 77, the Art of Scientific Computing*, 2nd ed. (Cambridge University Press, Cambridge, UK, 1992).
- [34] J. L. Egido and P. Ring, *Nucl. Phys. A* **388**, 19 (1982).
- [35] M. Borrajo, T. Rodriguez, and J. L. Egido, *Phys. Lett. B* **746**, 341 (2015).
- [36] N. Shimizu, T. Abe, M. Honma, T. Otsuka, T. Togashi, Y. Tsunoda, Y. Utsuno, and T. Yoshida, *Phys. Scripta* **92**, 063001 (2017); N. Shimizu, T. Abe, Y. Tsunoda, Y. Utsuno, T. Yoshida, T. Mizusaki, M. Honma, and T. Otsuka, *Prog. Theor. Exp. Phys.* **2012**, 01A205 (2012).
- [37] A. Poves, J. Sanchez-Solano, E. Caurier, and F. Nowacki, *Nucl. Phys. A* **694**, 157 (2001).
- [38] M. Honma, T. Otsuka, B. A. Brown and T. Mizusaki, *Eur. Phys. J. A* **25** (Suppl. 1), 499 (2005).
- [39] N. Shimizu, T. Mizusaki, Y. Utsuno, and Y. Tsunoda, *Comp. Phys. Commun.* **244**, 372 (2019).
- [40] N. Shimizu, Y. Utsuno, T. Mizusaki, T. Otsuka, T. Abe, and M. Honma, *Phys. Rev. C* **82**, 061305(R) (2010).
- [41] M. Horoi, B. A. Brown, and V. Zelevinsky, *Phys. Rev. C* **67**, 034303 (2003).
- [42] T. Hjelt, K. W. Schmid, and A. Faessler, *Nucl. Phys. A* **697**, 164 (2002).
- [43] T. Otsuka, M. Honma, and T. Mizusaki, *Phys. Rev. Lett.* **81**, 1588 (1998).
- [44] K. Heyde and J. L. Wood, *Rev. Mod. Phys.* **83**, 1467 (2011).
- [45] B. A. Brown, N. J. Stone, J. R. Stone, I. S. Towner, and M. Hjorth-Jensen, *Phys. Rev. C* **71**, 044317 (2005).
- [46] A. Gade, I. Wiedenhover, H. Meise, A. Gelberg, and P. von Brentano, *Nucl. Phys. A* **697**, 75 (2002).
- [47] A. Hayashi, K. Hara, and P. Ring, *Phys. Rev. Lett.* **53**, 337 (1984).
- [48] J. M. Yao, J. Meng, P. Ring, and D. Vretenar, *Phys. Rev. C* **81**, 044311 (2010).
- [49] Y. Tsunoda and T. Otsuka, *Phys. Rev. C* **103**, L021303 (2021).
- [50] L. Kaya, A. Vogt, P. Reiter *et al.*, *Phys. Rev. C* **100**, 024323 (2019).
- [51] K. Neergård and E. Wüst, *Nucl. Phys. A* **402**, 311 (1983).
- [52] J. Menendez, N. Hinohara, J. Engel, G. Martinez-Pinedo, and T. R. Rodriguez, *Phys. Rev. C* **93**, 014305 (2016).